

ARTICLE

<https://doi.org/10.1038/s42005-019-0219-4>

OPEN

Photoinduced possible superconducting state with long-lived disproportionate band filling in FeSe

Takeshi Suzuki ¹, Takashi Someya¹, Takahiro Hashimoto¹, Shoya Michimae¹, Mari Watanabe¹, Masami Fujisawa¹, Teruto Kanai¹, Nobuhisa Ishii¹, Jiro Itatani ¹, Shigeru Kasahara ², Yuji Matsuda ², Takasada Shibauchi ³, Kozo Okazaki ^{1,4} & Shik Shin ^{1,4}

Photoexcitation is a very powerful way to instantaneously drive a material into a novel quantum state without any fabrication, and variable ultrafast techniques have been developed to observe how electron, lattice, and spin degrees of freedom change. One of the most spectacular phenomena is photoinduced superconductivity, and it has been suggested in cuprates that the transition temperature T_c can be enhanced from the original T_c with significant lattice modulations. Here, we show a possibility for another photoinduced high- T_c superconducting state in the iron-based superconductor FeSe. The transient electronic state over the entire Brillouin zone is directly observed by time- and angle-resolved photoemission spectroscopy using extreme ultraviolet pulses obtained from high harmonic generation. Our results of dynamical behaviors from 50 fs to 800 ps consistently support the favourable superconducting state after photoexcitation well above T_c . This finding demonstrates that multiband iron-based superconductors emerge as an alternative candidate for photoinduced superconductors.

¹Institute for Solid State Physics, The University of Tokyo, Kashiwa, Chiba 277-8581, Japan. ²Department of Physics, Kyoto University, Kyoto 606-8502, Japan. ³Department of Advanced Materials Science, The University of Tokyo, Kashiwa, Chiba 277-8561, Japan. ⁴AIST-UTokyo Advanced Operando-Measurement Technology Open Innovation Laboratory (OPERAND-OIL), Kashiwa, Chiba 277-8581, Japan. Correspondence and requests for materials should be addressed to T.S. (email: takeshi.suzuki@issp.u-tokyo.ac.jp) or to K.O. (email: okazaki@issp.u-tokyo.ac.jp) or to S.S. (email: shin@issp.u-tokyo.ac.jp)

Among Fe-based superconductors, FeSe has attracted enormous interest owing to the absence of anti-ferromagnetism, in contrast to other Fe-based superconductors. Moreover, FeSe has potential superiority in exhibiting a higher critical temperature (T_c) of superconductivity under various external applications. Although T_c is only ~ 10 K at ambient pressure¹, a significant increase in T_c to ~ 40 K by physical pressure has been achieved^{2–4}. Regarding fabrications, the intercalation of a spacer layer can increase T_c to ~ 40 K^{5,6}, and the T_c of single-layer FeSe has been reported to be ~ 60 K⁷. The key ingredient for achieving higher T_c values lies in the band-structure design. For example, the dramatic increase in T_c for single-layer FeSe is accompanied by the disappearance of the hole Fermi surface (FS) and the increase in the electron FS⁷. In this context, photoexcitation has substantial advantages over other methods because it can instantaneously manipulate a material of interest in situ without any fabrication^{8–10}. One of the striking phenomena is the photoinduced superconductivity reported in high- T_c cuprate superconductors, where the key mechanism is the lattice modulation¹¹. Furthermore, it should be emphasized that near-infrared pulses have also been employed for excitation, which initially excite the electronic system, while mid-infrared pulses can resonantly excite the lattice system^{12,13}.

Recently, photoexcited phenomena for Fe-based superconductors have been intensively studied. In photoexcited BaFe₂As₂, the temporally periodic formation of spin-density waves was observed by terahertz (THz) spectroscopy¹⁴. The demonstration of chemical potential control¹⁵ and the possibility of photoinduced superconductivity¹⁶ were reported by time- and angle-resolved photoemission spectroscopy (ARPES). The key mechanism is the connection of the electron and spin properties to the lattice motion, and each report is discussed in terms of the clear appearance of coherent phonons^{17,18}. In photoexcited FeSe, coherent phonons were also reported by ARPES¹⁹, and the connection between the dynamical band shift and lattice dynamics was directly measured by combining ARPES and time-resolved X-ray diffraction²⁰. However, an important but lacking aspect in photoexcited FeSe is the dynamic properties of the electron pockets located around the Brillouin zone (the M point). By directly observing how the hole and electron pockets change by photoexcitation, we can also gain insight into the response of the lattice degree of freedom in the photoexcited state. Because it is relatively easy to set up, a photon energy of 6 eV is typically employed for ARPES measurements. However, due to the lack of photon energy, ARPES under 6 eV cannot access the M point. This is overcome by using high harmonic generation (HHG) to obtain higher photon energy and capture a larger region of the Brillouin zone²¹.

Here, we investigate the nonequilibrium electronic structure of FeSe by performing ARPES using an extreme ultraviolet (XUV) laser. Oscillations as a result of A_{1g} coherent phonon excitation are clearly observed for both the hole and electron FSs, and they are found to be in phase with each other, the behavior of which is different from that of BaFe₂As₂¹⁶. From long-delay time measurements, we elucidate that the disproportionate band filling between the hole and electron bands persists for longer than 800 ps. Interestingly, this state mimics the electronic structure of a single-layer FeSe. Furthermore, the additional LEM found in both the hole and electron FSs is ascribed to the superconducting gap. By comparing with band-structure calculations, we find that the distance between the neighboring Se and Fe layers increases in the photoexcited metastable state. This result suggests that fairly long-lived nonequilibrium electronic and lattice structures are available by photoexcitation in FeSe, owing to its indirect semi-metallic band structure. We propose that a long-lived photo-induced superconducting state could be expected for FeSe.

Results

Displacive excitation of coherent phonons. Figure 1a shows an illustration of our experimental setup for the ARPES measurements. To characterize the cleaved surfaces, we first performed conventional static ARPES using a He discharge lamp (21.2 eV). Figure 1b shows the result of FS mapping, and two FSs are clearly seen around the Γ (0, 0) and M (π , π) points. Figure 1c, d shows the ARPES intensity as a function of energy and momentum taken at around the Γ and M points, respectively. The horizontal momentum axis corresponds to the solid lines in Fig. 1b, while the vertical energy axis corresponds with respect to the Fermi level (E_F). Hole and electron dispersions are observed around the Γ and M points, respectively. The results are consistent with previous reports²². All spectra were taken at 15 K in this work.

Figure 2a, b shows the momentum-integrated ARPES intensity measured across the hole and electron FSs, with pump fluences of 2.45 and 2.28 mJ cm⁻², respectively, as a function of the pump–probe delays (Δt). All the measurements in this work are performed under the condition in which the space charge effects are minimized. Due to the low efficiency of the HHG process, the energy resolution is set to 250 meV. The integrated range is along the orange-solid and green-solid lines shown in Fig. 1b for the hole and electron FSs, respectively. After intense pulse excitation, electrons are immediately excited above E_F , followed by relatively slow relaxation dynamics at both FSs. To see the photoexcited dynamics more clearly, we show in Fig. 2c, d an integrated intensity above E_F corresponding to the regions surrounded by green boxes in Fig. 2a, b, respectively. Overall, immediate excitation and overshooting decay at $\Delta t = 0$ ps followed by relatively slow recovery dynamics are observed, reflecting the carrier dynamics. In addition, oscillatory behaviors are clearly observed superimposed onto the background carrier dynamics. These oscillatory components are especially evident at the initial time ($\Delta t < 1.5$ ps). At later times of approximately $\Delta t = 3$ ps, it should be noted that they exhibit a contrasting feature, i.e., the photoemission intensity decreases at the hole FS, while the intensity at the electron FS increases. This behavior is also confirmed in the time- and angle-resolved photoemission spectra shown in Supplementary Fig. 1 as the downward band shifts at the Γ point as well as the increase in electrons in the electron pockets at the M point. These signatures will be discussed later in more detail. To highlight the oscillatory components, we first fit the background carrier dynamics with two-component exponential decay functions convoluted with a Gaussian. They are shown by the black solid lines in Fig. 2c, d and were subtracted from the experimental data. The oscillatory components are displayed in Fig. 2e, f, respectively. These oscillations are in phase with each other and cosine-like, with a frequency of 5.3 THz. From the comparison with Raman spectra²³, this oscillation frequency is assigned to the A_{1g} phonon mode, in which two Se layers oscillate symmetrically with respect to the sandwiched Fe layer. The recent results of Raman spectroscopy performed on single-crystal FeSe revealed the frequency of the A_{1g} phonon mode to be 5.5 THz, which justifies the assignment of the coherent phonon observed in the previous ARPES studies^{19,20}. Moreover, the fast Fourier transforms (FFTs) of the oscillatory components are shown in Fig. 2g, and the FFT peak amplitudes for both the hole and electron FSs significantly increase as a function of the pump fluence shown in Fig. 2h. These cosine-like and intensity-dependent behaviors confirm that the observed oscillations are attributed to the displacive excitation of coherent phonons (DECP)²⁴. According to the DECP mechanism, photoexcitation moves the system to a free-energy curve of excited states with a minimum position at different \hbar from the equilibrium state. As a result, Se atoms simultaneously oscillate with a center at the new stable (metastable) position. Since the oscillatory components of

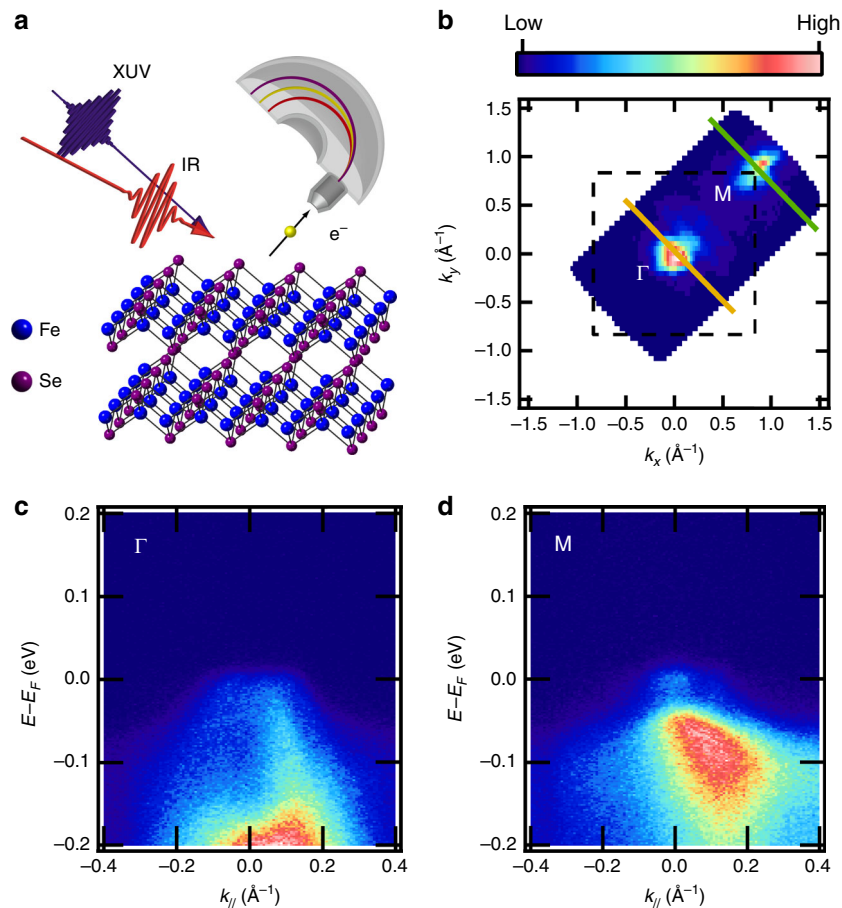


Fig. 1 Schematics and conventional angle-resolved photoelectron spectroscopy (ARPES). **a** Schematics of time- and angle-resolved photoemission spectroscopy (TARPES) for FeSe. An infrared (IR) pulse of 1.55 eV is used for the pump, and an extreme ultraviolet (XUV) pulse of 27.9 eV by high harmonic generation from Ar gas is used for the probe to cover a large area including the M point. **b** Fermi surface mapping of FeSe. The intensity is mapped onto the in-plane electron momentum (k_x, k_y). Orange and green lines represent measured cuts at the Γ and M points for the TARPES measurements, respectively. Black dashed lines indicate the Brillouin zone boundary. **c, d** Band dispersions at the Γ and M points along the momentums shown in **(b)**. The vertical axes are represented as electron energies (E) with respect to the Fermi levels (E_F). Spectra in **b-d** were measured by a He-discharge lamp at 21.2 eV

the photoemission intensity above E_F reflect the size of FSs¹⁶, the cosine-like signature indicates that the photoinduced metastable state is toward smaller FSs for the hole and electron pockets.

Long-lived charge disproportionate state. As briefly observed, the photoemission intensity exhibits contrasting features between the hole and electron FSs at a larger delay time ($\Delta t = 3$ ps). This feature also persists at a relatively long-delay time, as shown in Supplementary Fig. 2. To investigate this behavior in more detail, we analyzed energy distribution curves (EDCs) for slow dynamics. Figure 3a presents the EDCs before ($\Delta t = -30$ ps) and after ($\Delta t = 110$ and 810 ps) the arrival of pump pulses for the hole FS, while the result for the electron FS is shown in Fig. 3b. The pump fluences for the hole and electron bands are 2.45 and 2.28 mJ cm^{-2} , respectively. After photoexcitation, the EDCs for both the hole and electron FSs become significantly broader at $\Delta t = 0.16$ ps, yet return soon at $\Delta t = 3.24$ ps to almost the same as those at 110 and 810 ps. This indicates that the electronic temperature is well cooled. Regarding the shift of the EDCs, the clear one toward the lower-energy side is noticed at the hole FS. On the other hand, at the electron FS (Fig. 3b), the EDC intensities for $\Delta t = 110$ and 810 ps around $E - E_F = -0.1$ eV are reduced, while no clear shift appears. For quantitative insights, we evaluate the shift of the leading-edge midpoint (LEM). Figure 3c shows the temporal

LEM shifts. As clearly shown, the LEM shift at the hole FS is negative, while that at the electron FS is negligibly small. In other words, the temporal band filling is disproportionate between the hole and electron bands. Interestingly, the photoexcited electronic structure mimics that of the monolayer FeSe film, in which only electron FSs are observed⁷. Furthermore, this disproportionate band filling persists longer than the measured delay time of ~ 800 ps. This long lifetime of carriers can be ascribed to the indirect semimetallic band structures, where the electron-hole recombination must accompany the assistance of phonons with a large momentum^{25,26}. Figure 3d shows the LEM shift as a function of the pump fluence, in which the values and estimated errors are the averages and standard deviations in $\Delta t > 0$, respectively. The trend of the disproportionality between the hole and electron bands, as illustrated in Fig. 3e, becomes more evident with increasing pump fluence. However, it should be noted that the negative shift of the LEM for the hole FSs is not equal to the positive shift for the electron FSs, and this signature is more pronounced for higher fluence.

Photoinduced superconductivity. In the single-hole and electron-band picture, photoexcited electrons are relaxed to the electron bands after the relatively fast processes of multiple electron-electron and electron-phonon scatterings. If the density

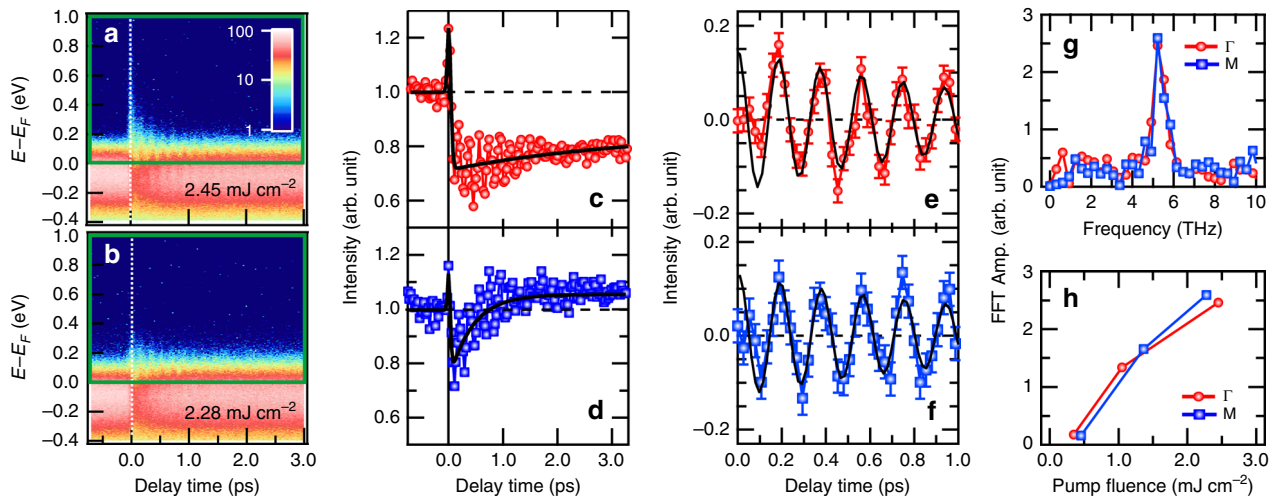


Fig. 2 Time- and angle-resolved photoemission spectra and oscillation behavior. **a, b** Time-resolved photoemission spectra taken around the Γ and M points, respectively. The vertical axes are represented as electron energies (E) with respect to the Fermi levels (E_F). **c, d** Integrated photoemission intensity above the Fermi level corresponding to the region surrounded by green boxes in **(a)** and **(b)**, respectively. **e, f** Oscillatory components at the Γ and M points. They are obtained by subtracting the carrier dynamics from **c** and **d**. Errors bars are estimated as standard deviations of the intensities before the arrival of the pump. Oscillations are in phase between the Γ and M points, as clearly shown by the black dashed lines. **g** Amplitude of the fast Fourier transformation of **(e)** and **(f)**. Both of them show peak structures at 5.3 THz. **h** Fast Fourier transformation (FFT) amplitudes at 5.3 THz for the Γ and M points as a function of the pump fluence

of states is similar between the hole and electron FSs, the LEM shift should be the same amount with the opposite sign. Hence, it should be unusual for the LEM shift at the electron FS to be negatively small for a higher fluence. If the overall shift of E_F is included in these LEM shifts, one possibility is due to the surface photovoltage (SPV) effect²⁷. However, it is not expected to occur in a semimetallic system such as FeSe because the SPV effect is typically induced by the surface band bending of semiconductors. Another possibility is a multiphoton effect due to the strong excitation by a near-infrared pump²⁸. Since we confirmed the absence of photoelectron intensities due to a multiphoton effect by measuring no signal with only pump pulses, this explanation can also be unlikely. The Floquet band theory may also explain our results, in which many replica bands appear apart from the original band by the photon energy used for excitation. Although the Floquet band theory significantly changes the band structure, the reported Floquet states have a relatively shorter lifetime around <1 ps^{29–31}. Because our main focus in this work is LEM shifts at times later than 100 ps, we have concluded that our results are less likely to be explained by the Floquet band theory. After considering all these effects, the overall LEM shifts can be ascribed to a gap originating from some orders.

To identify superconducting signatures more explicitly, we extract the averaged photoinduced superconducting gap, Δ , shown as a black solid line and markers in Fig. 3d, which is given by the following relationship:

$$\Delta = -\frac{m_h \text{LEM}_h + m_e \text{LEM}_e}{m_h + m_e}, \quad (1)$$

where m_h and m_e are the effective masses of the hole and electron pockets, respectively. Their ratio is $m_h/m_e = 4/3$ ³². LEM_h and LEM_e are LEM shifts for the hole and electron pockets, respectively. A detailed description of how to extract the averaged superconducting gap is found in the Supplementary Discussion. Considering that superconductivity coexists with the orbital ordering under equilibrium for FeSe, but the orbital ordering induces no bandgap but a band splitting, the photoinduced superconducting gap is the most plausible origin. The mechanism

of the stabilization of the superconducting state due to the dispersive excitation is explained in the next section.

Lattice modulation induced by dispersive excitations. To determine whether h becomes higher or lower in the photo-induced metastable state¹⁸, we performed band-structure calculations based on density functional theory (DFT). The results of the band-structure calculations are found in Supplementary Fig. 3²⁹. Figure 4a–c shows the calculated FSs for the two hole bands ($yz/zx(\text{odd})$ and $yz/zx(\text{even})$) and the electron band. Because the DFT calculations for FeSe cannot provide quantitative agreement with the measured band dispersions^{22,33,34}, band-dependent shifts of -0.08 and $+0.17$ eV, as well as renormalization with factors of 3 and 2, are introduced for the electron and hole bands, respectively. The equilibrium state is shown as the dotted lines, whereas the $+5\%$ and -5% changes in h are shown as the solid and dashed lines, respectively. Since the probe pulses are polarized along the detector slit in this work, the contribution to the photoemission intensity around the Γ point has been reported to be mainly from the $yz/zx(\text{even})$ orbital due to the photoemission matrix element^{22,34}. In each band, the FS shrinks as h increases. From the comparison between the experiments and calculations, a higher h is interpreted to be realized in the photoinduced metastable state, as illustrated by the yellow arrows in Fig. 4d. This trend agrees with the previous report measuring the band shift at the Γ point by high-energy-resolution TARPES²⁰, where the initial dynamics of the downward band shift are revealed to be synchronized with the increase in h . Although a quantitative agreement is difficult to achieve between the DFT calculations and the measured band dispersions, the trend of the band shifts with respect to the change in h should be correct, as reported previously²⁰, the authors of which directly measured the dynamics of band dispersions as well as lattice distortions and compared them with DFT + DMFT calculations. Although our method using DFT calculations is less quantitative for reproducing the measured band dispersions than the DFT + DMFT calculations, the fact that both methods predict the same tendency with respect to the change in h strongly suggests that

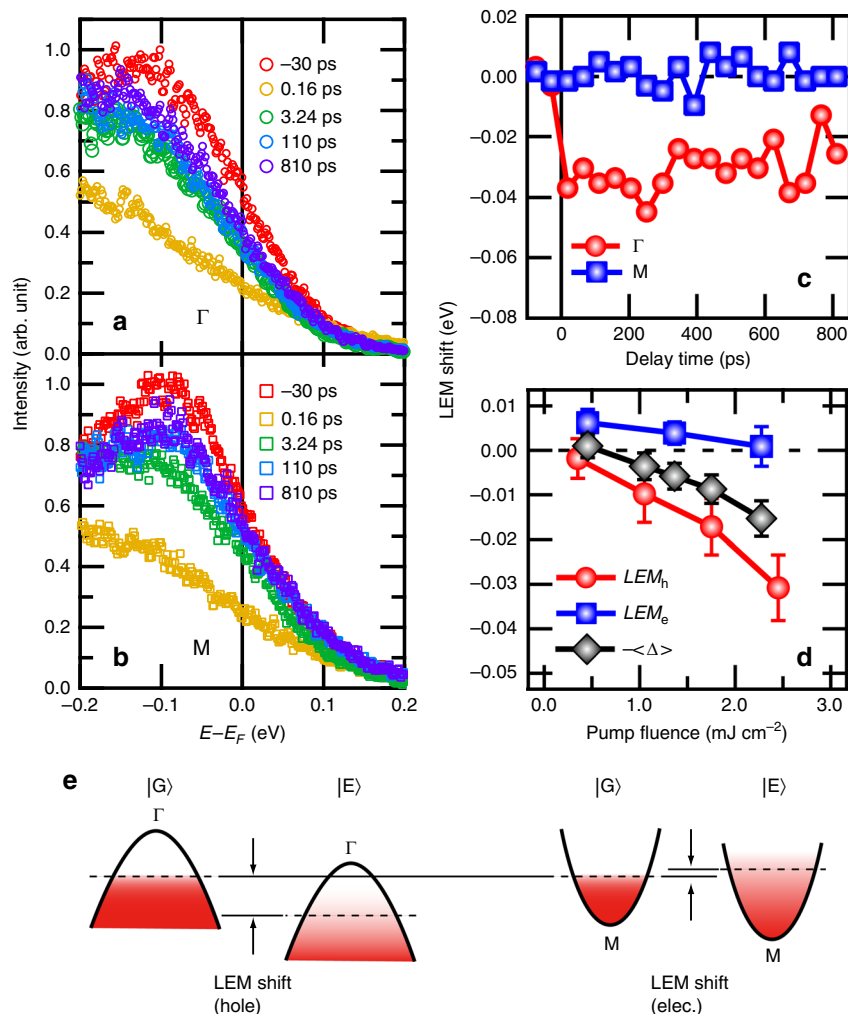


Fig. 3 Energy distribution curves and shifts of the leading-edge midpoint. **a, b** Energy distribution curves (EDCs) for Γ and M points at representative delay times with pump fluences of 2.45 and 2.28 mJ/cm^2 , respectively. Shifts of the leading-edge midpoint (LEM) as a function of time (**c**) and pump fluence (**d**) at hole (Γ) and electron (M) bands. In Fig. 3d, the averaged superconducting gap, $\langle \Delta \rangle$, is shown as black solid lines and markers. Because $\langle \Delta \rangle$ negatively contributes to the LEM shifts, we plot $-\langle \Delta \rangle$ in Fig. 3d for LEM_h and LEM_e are estimated as standard deviations after the arrival of the pump, and that for $\langle \Delta \rangle$ is obtained via the relationship of Eq. (1). **e** Illustration of photoinduced LEM shifts for hole (Γ) and electron (M) bands. $|G\rangle$ and $|E\rangle$ represent the ground and photoexcited states, respectively

our DFT calculation results should also predict the same tendency.

Discussion

Regarding superconductivity, it has been reported that T_c increases with higher h by physical pressure⁴. Photoexcitation can induce the same tendency as the physical pressure and can be another tool for the enhancement of the superconductivity. Successive recent reports on the photoinduced superconductivity in cuprate superconductors have discussed the important role of lattice motions^{11,35}. For the excitation employed in most studies, a mid-infrared pulse is used to resonantly excite the lattice degree of freedom (phonons). However, the eventual lattice modulation playing a decisive role in photoinduced superconductivity was found to be the Raman-active A_g phonon, which is nonlinearly coupled to the photoexcited infrared-active phonon mode¹¹. Thus, it is indicated that the important mechanism relies on how to access the A_g lattice modulation that is favorable for the superconductivity. Interestingly, near-infrared pulses are also used for excitation, which initially excite the electronic degree of freedom. Although the precise mechanism is still under debate, it is proposed that the lattice modulation is induced by the change

in the distribution of the electronic system³⁶, which is very similar to our situation.

Along with cuprate superconductors, Fe-based superconductors can be an alternative candidate for photoinduced superconductivity because the pronounced lattice motions are detected by coherent phonons, and interestingly, the present results of higher h in FeSe are favorable for superconductivity. A long-lived aspect of the photoinduced phase owing to the indirect semimetallic band structures is also a characteristic feature for Fe-based superconductors compared with a short-lived feature for cuprate superconductors due to direct single-band structures.

In summary, we have investigated the photoexcited electron dynamics of the hole and electron FSs in FeSe by TARPES using the HHG technique. We have proposed that the ultrafast optical technique can offer another route to create new long-lived electronic and lattice structures in FeSe as a consequence of its indirect semimetallic band structure.

Method

Time- and angle-resolved photoemission spectroscopy. TARPES is a pump-probe-type measurement, where both pulses are originally generated from a Ti:Sapphire amplification system with a repetition rate of 1 kHz and a pulse

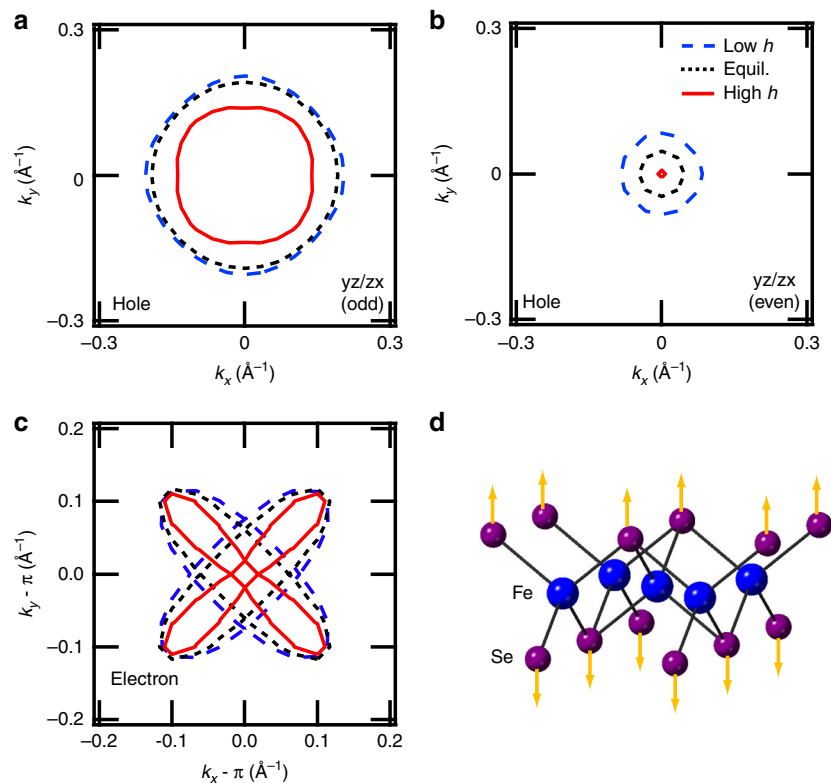


Fig. 4 Calculated Fermi surfaces with varying Se height. **a** Fermi surface of the hole yz/zx (odd) band calculated by density functional theory with generalized gradient approximation (DFT-GGA) for different Se heights (h). The equilibrium state is shown as a dotted line, whereas the +5% and -5% changes in h are shown as solid and dashed lines, respectively. The Fermi surfaces are plotted in the in-plane momentum (k_x , k_y). The results for the hole yz/zx (even) and electron bands are shown in **(b, c)**, respectively. **d** Illustration of lattice modulation by photoexcitation. After photoexcitation, the Se positions move toward larger h directions, shown as yellow arrows

duration of 35 fs. A near-infrared (NIR) pulse (1.55 eV) is used for the pump, while XUV pulses (27.9 eV) are used for the probe. XUV pulses are obtained by selecting the ninth-order harmonic generated from argon gas by using a double-frequency pulse (3.10 eV). The time resolution is measured to be ~ 80 fs from the cross-correlation measurement between the pump and probe pulses, and the energy resolution is set to 250 meV. Photoemission spectra are measured by using a Scienta R4000 hemispherical electron analyzer.

Sample. High-quality single crystals of FeSe were grown by the chemical vapor transport method by using KCl/AlCl₃ as a transport agent³⁷. Clean surfaces were obtained by cleaving in situ.

Band-structure calculations. Band-structure calculations based on density functional theory (DFT) were performed by using a WIEN2k package³⁸. $a = 3.7707$ \AA , $c = 5.521$ \AA , and $h = 1.4723$ \AA , where h is the Se height from the Fe layer, were used for the lattice parameters in the equilibrium state³⁷.

Data availability

The data supporting the findings of this study are available from the corresponding author upon request.

Received: 22 January 2019 Accepted: 21 August 2019

Published online: 25 September 2019

References

- Kasahara, S. et al. Field-induced superconducting phase of FeSe in the BCS-BEC cross-over. *Proc. Natl Acad. Sci. USA* **111**, 16309 (2014).
- Medvedev, S. et al. Electronic and magnetic phase diagram of β -Fe_{1.01}Se with superconductivity at 36.7 K under pressure. *Nat. Mater.* **8**, 630 (2010).
- Sun, J. P. et al. High- T_c superconductivity in FeSe at high pressure: dominant hole carriers and enhanced spin fluctuations. *Phys. Rev. Lett.* **118**, 147004 (2017).
- Matsura, K. et al. Maximizing T_c by tuning nematicity and magnetism in FeSe_{1-x}S_x superconductors. *Nat. Commun.* **8**, 1038 (2017).
- Burrard-Lucas, M. et al. Enhancement of the superconducting transition temperature of FeSe by intercalation of a molecular spacer layer. *Nat. Mater.* **12**, 15 (2013).
- Lu, X. F. et al. Coexistence of superconductivity and antiferromagnetism in (Li_{0.8}Fe_{0.2})OHFeSe. *Nat. Mater.* **14**, 325 (2015).
- He, S. et al. Phase diagram and electronic indication of high-temperature superconductivity at 65 K in single-layer FeSe films. *Nat. Mater.* **12**, 605 (2013).
- Miyano, K., Tanaka, T., Tomioka, Y. & Tokura, Y. Photoinduced insulator-to-metal transition in a perovskite manganite. *Phys. Rev. Lett.* **78**, 4257–4260 (1997).
- Fausti, D. et al. Light-induced superconductivity in a stripe-ordered cuprate. *Science* **331**, 189 (2011).
- Matsunaga, R. et al. Higgs amplitude mode in the BCS superconductors Nb_{1-x}Ti_xN induced by terahertz pulse excitation. *Phys. Rev. Lett.* **111**, 057002 (2013).
- Mankowsky, R. et al. Nonlinear lattice dynamics as a basis for enhanced superconductivity in YBa₂Cu₃O_{6.5}. *Nature* **516**, 71 (2014).
- Nicoletti, D. et al. Optically induced superconductivity in striped La_{2-x}Ba_xCuO₄ by polarization-selective excitation in the near infrared. *Phys. Rev. B* **90**, 100502 (R) (2014).
- Casandruc, E. et al. Wavelength-dependent optical enhancement of superconducting interlayer coupling in La_{1.885}Ba_{0.115}CuO₄. *Phys. Rev. B* **91**, 174502 (2015).
- Kim, K. W. et al. Ultrafast transient generation of spin-density-wave order in the normal state of BaFe₂As₂ driven by coherent lattice vibrations. *Nat. Mater.* **11**, 497 (2012).
- Yang, L. X. et al. Ultrafast modulation of the chemical potential in BaFe₂As₂ by coherent phonons. *Phys. Rev. Lett.* **112**, 207001 (2014).
- Okazaki, K. et al. Antiphase Fermi-surface modulations accompanying displacement excitation in a parent compound of iron-based superconductors. *Phys. Rev. B* **97**, 121107 (R) (2018).
- Rettig, L. et al. Ultrafast structural dynamics of the Fe-pnictide parent compound BaFe₂As₂. *Phys. Rev. Lett.* **114**, 067402 (2015).
- Gerber, S. et al. Direct characterization of photoinduced lattice dynamics in BaFe₂As₂. *Nat. Commun.* **6**, 7377 (2015).

19. Yang, S. et al. Thickness-dependent coherent phonon frequency in ultrathin FeSe/SrTiO₃ films. *Nano Lett.* **15**, 4150 (2015).
20. Gerber, S. et al. Femtosecond electron-phonon lock-in by photoemission and x-ray free-electron laser. *Science* **357**, 71 (2017).
21. Rohwer, T. et al. Collapse of long-range charge order tracked by time-resolved photoemission at high momenta. *Nature* **471**, 490 (2011).
22. Shimojima, T. et al. Lifting of *xz/yz* orbital degeneracy at the structural transition in detwinned FeSe. *Phys. Rev. B* **90**, 121111 (R) (2014).
23. Kumar, P. et al. Anomalous Raman scattering from phonons and electrons of superconducting FeSe_{0.82}. *Solid State Commun.* **150**, 557 (2010).
24. Zeiger, H. J. et al. Theory for dispersive excitation of coherent phonons. *Phys. Rev. B* **45**, 768 (1992).
25. Lopez, A. A. Electron-Hole Recombination in Bismuth. *Phys. Rev.* **175**, 823 (1968).
26. Sheu, Y. M., Chien, Y. J., Uher, C., Fahy, S. & Reis, D. A. Free-carrier relaxation and lattice heating in photoexcited bismuth. *Phys. Rev. B* **87**, 075429 (2013).
27. Yang, S.-L., Sobota, J. A., Kirchmann, P. S. & Shen, Z.-X. Electron propagation from a photo-excited surface: implications for time-resolved photoemission. *Appl. Phys. A* **116**, 85 (2014).
28. Oloff, L.-P. et al. Pump laser-induced space-charge effects in HHG-driven time- and angle-resolved photoelectron spectroscopy. *J. Appl. Phys.* **119**, 225106 (2016).
29. Wang, Y. H., Steinberg, H., Jarillo-Herrero, P. & Gedik, N. Observation of Floquet-Bloch states on the surface of a topological insulator. *Science* **342**, 453 (2013).
30. Mahmood, F. et al. Selective scattering between Floquet-Bloch and Volkov states in a topological insulator. *Nat. Phys.* **12**, 306 (2016).
31. Liu, R. et al. Femtosecond to picosecond transient effects in WSe₂ observed by pump-probe angle-resolved photoemission spectroscopy. *Sci. Rep.* **7**, 15982 (2017).
32. Watson, M. D. et al. Emergence of the nematic electronic state in FeSe. *Phys. Rev. B* **91**, 155106 (2015).
33. Nakayama, K. et al. Angle-resolved photoemission spectroscopy of the iron-chalcogenide superconductor Fe_{1.03}Te_{0.7}Se_{0.3}: strong coupling behavior and the universality of interband scattering. *Phys. Rev. Lett.* **105**, 197001 (2010).
34. Maletz, J. et al. Unusual band renormalization in the simplest iron-based superconductor FeSe_{1-x}. *Phys. Rev. B* **89**, 220506 (R) (2014).
35. Kaiser, S. Light-induced superconductivity in high-*T_c* cuprates. *Phys. Scr.* **92**, 103001 (2017).
36. Zhang, S. J. et al. Light-induced new collective modes in the superconductor La_{1.905}Ba_{0.095}CuO₄. *Phys. Rev. B* **98**, 020506 (R) (2018).
37. Böhmer, A. E. et al. Lack of coupling between superconductivity and orthorhombic distortion in stoichiometric single-crystalline FeSe. *Phys. Rev. B* **87**, 180505 (R) (2013).
38. Blaha, P., Schwarz, K., Madsen, G. K. H., Kvasnicka, D. & Luitz, J. *WIEN2K, An Augmented Plane Wave + Local Orbitals Program for Calculating Crystal Properties* (Karlheinz Schwarz, Techn. Universität Wien, Austria, 2001).

Acknowledgements

This work was supported by Grants-in-Aid for Scientific Research (KAKENHI) (Grant numbers JP18K13498, JP19H00659, JP19H01818, and JP19H00651) from the Japan Society for the Promotion of Science (JSPS) and by JSPS KAKENHI on Innovative Areas “Quantum Liquid Crystals” (Grant Numbers JP19H05824 and JP19H05826), and by Quantum Leap Flagship Program (Q-LEAP) (Grant number JPMXS0118068681) from the Ministry of Education, Culture, Sports, Science, and Technology (MEXT). T. H. acknowledges the JSPS Research Fellowship for Young Scientists (DC2) and financial support from JSPS through the program for Leading Graduate School (Materials Education Program for the Future Leaders in Research, Industry, and Technology).

Author contributions

T. Suzuki, T. Someya, T.H., S.M., M.W. and K.O. performed the TARPES measurements. T. Suzuki performed the data analysis. M.F., T.K., N.I. and J.I. conducted maintenance of the HHG laser system and improvements of the TARPES apparatus. S.K., Y.M. and T. Shibauchi grew high-quality single crystals and characterized them. T. Suzuki, Y.M., T. Shibauchi and K.O. wrote the paper. K.O. and S.S. designed the project. All the authors discussed the results and contributed to the paper.

Additional information

Supplementary information accompanies this paper at <https://doi.org/10.1038/s42005-019-0219-4>.

Competing interests: The authors declare no competing interests.

Reprints and permission information is available online at <http://npg.nature.com/reprintsandpermissions/>

Publisher's note Springer Nature remains neutral with regard to jurisdictional claims in published maps and institutional affiliations.



Open Access This article is licensed under a Creative Commons Attribution 4.0 International License, which permits use, sharing, adaptation, distribution and reproduction in any medium or format, as long as you give appropriate credit to the original author(s) and the source, provide a link to the Creative Commons license, and indicate if changes were made. The images or other third party material in this article are included in the article's Creative Commons license, unless indicated otherwise in a credit line to the material. If material is not included in the article's Creative Commons license and your intended use is not permitted by statutory regulation or exceeds the permitted use, you will need to obtain permission directly from the copyright holder. To view a copy of this license, visit <http://creativecommons.org/licenses/by/4.0/>.

© The Author(s) 2019